

## Supporting Information

### Bi-facial Stamping for High Efficiency Perovskite Solar Cells

Yong Zhang<sup>a†</sup>, Seul-Gi Kim<sup>a†</sup>, Donghwa Lee<sup>b</sup>, Hyunjung Shin<sup>c</sup>, Nam-Gyu Park<sup>a\*</sup>

<sup>a</sup>School of Chemical Engineering, Sungkyunkwan University, Suwon 440-746, Korea.

<sup>b</sup>Department of Materials Science and Engineering, and Division of Advanced Materials Science, Pohang University of Science and Technology (POSTECH), Pohang 37673, Korea

<sup>c</sup>Department of Energy Science, Sungkyunkwan University, Suwon 440-746, Korea

<sup>†</sup>These authors contributed equally to this work.

\* Corresponding author. E-mail: npark@skku.edu

#### Experimental Section

**Synthesis of  $CH_3NH_3I$ :** Methylammonium iodide (MAI,  $CH_3NH_3I$ ) was synthesized by reacting 27.8 mL of  $CH_3NH_2$  (40 wt% in methanol, TCI) with 30 mL of hydroiodic acid (57 wt% in water, Aldrich) in a round-bottomed flask in an ice bath for 2 h with magnetic stirring. The precipitates were recovered by evaporating at 50 °C for 1 h using rotary evaporator. Resulting product was dissolved in ethanol and recrystallized by diethyl ether for three times, and then finally dried at 50 °C in the vacuum oven for 24 h and then stored in Ar filled glove box. All the chemicals were used as-received without further purification.

**Synthesis of  $HC(NH_2)_2I$ :** Formamidinium iodide (FAI,  $HC(NH_2)_2I$ ) was synthesized by reacting 15 g of formamidinium acetate (99%, Aldrich) with 30 mL of hydroiodic acid in a

round-bottomed flask in an ice bath for 2 h. Dark yellow precipitate was recovered by evaporating at 60 °C for 1 h. Resulting product was dissolved in ethanol and recrystallized in diethyl ether for three times. The final white precipitate was dried at 50 °C in the vacuum oven for 24 h and then stored in Ar filled glove box.

**Synthesis of  $CH_3NH_2CH_3I$ :** Ethylammonium iodide (EAI,  $CH_3CH_2NH_3I$ ) was synthesized by reacting 20 mL of ethylamine (2.0 M in methanol, Aldrich) and 6 mL of hydroiodic acid in a round-bottomed flask at 0 °C for 2 h. The precipitate was collected by evaporation at 50 °C for 1 h, which is followed by be dissolved in ethanol and recrystallized in diethyl ether for three times. Then finally dried at 50°C in a vacuum oven for 24 h and stored in Ar filled glove box.

**Solar cell fabrication:** Fluorine doped tin oxide (FTO) coated conductive glasses (Pilkington, TEC-8, 8  $\Omega$ /sq) were cleaned by detergent, followed by ultrasonic treatment in ethanol for 20 min and UV/Ozone (UVO) treatment for 20 min. UVO treatment was again conducted for 15 min prior to use. We have fabricated two types of perovskite solar cells: Normal mesoscopic structure with a thin  $TiO_2$  layer and mesoporous  $TiO_2$  layer and planar structure with a thin  $SnO_2$  layer. For the normal mesoscopic structure, the thin  $TiO_2$  film as a hole blocking layer (bl- $TiO_2$ ) was fabricated by immersing FTO glass in 20 mM  $TiCl_4$  aqueous solution (Sigma-Aldrich, > 98%) at 90 °C for 20 min, followed by annealing at 125 °C for 10 min. Homemade nanocrystalline  $TiO_2$  (average particle size of about 50 nm) paste was diluted in 1-butanol (1 g/10 mL), which was spin-coated on the bl- $TiO_2$  film at 2000 rpm for 20 s to form a mesoporous  $TiO_2$  (mp- $TiO_2$ ) layer. The spin-coated mp- $TiO_2$  layer was annealed at

125 °C for 5 min on a hot plate and then at 550 °C for 1 h in a muffle furnace. The annealed mp-TiO<sub>2</sub> film was post-treated with 20 mM TiCl<sub>4</sub> aqueous solution at 90 °C for 10 min, which was again annealed at 500 °C for 30 min. For the planar structure, the SnO<sub>2</sub> film was fabricated by spin-coating the commercial SnO<sub>2</sub> colloidal solution (Alfa Aesar, 15% in H<sub>2</sub>O), diluted to 4 wt%, at 4000 rpm for 20 s, which was annealed at 180 °C on hotplate for 30 min. The precursor solution for the MAPbI<sub>3</sub> layer was prepared by mixing 461 mg PbI<sub>2</sub> (TCI, 99.99%), 159 mg MAI and 71 μL of N,N'-dimethyl sulfoxide (DMSO) (>99.5%, Sigma) (molar ratio 1:1:1) in 521 μL of N,N'-dimethylformamide (DMF) (anhydrous, 99.8% Sigma-Aldrich). The precursor solution for the FAPbI<sub>3</sub> layer was prepared by mixing 461 mg PbI<sub>2</sub>, 172 mg FAI and 71 μL DMSO in 600 μL DMF (molar ratio 1:1:1). The precursor solution for the EAPbI<sub>3</sub> layer was prepared by mixing 461 mg PbI<sub>2</sub>, 173 mg EAI and 71 μL DMSO in 600 μL DMF (molar ratio 1:1:1). Perovskite films were fabricated using the Lewis acid-base adduct method according to our report.<sup>S1</sup> The perovskite solutions were spin-coated at 4000 rpm for 20 s and 0.5 mL diethyl ether was dripped on the rotating substrate (10 s after spinning) to obtain adduct films. For face-to-face perovskite film stamping, MAPbI<sub>3</sub>-coated substrate and FAPbI<sub>3</sub> (or EAPbI<sub>3</sub>)-coated substrate were separately prepared. The FAPbI<sub>3</sub> (or EAPbI<sub>3</sub>) coated substrate was first prepared by annealing at 100 °C for 1.5 min and then the MAPbI<sub>3</sub> coated substrate was prepared by annealing at 65 °C for 1 min without interval. The pre-annealed MAPbI<sub>3</sub> film was directly put on the FAPbI<sub>3</sub> film without pressure, which was annealed at 100 °C on hot plate for 9 min. Care should be taken in placing the MAPbI<sub>3</sub> film at the top and the FAPbI<sub>3</sub> (or EAPbI<sub>3</sub>) film at the bottom during stamping process (see Figure 1 in main text). After stamping two films were detached. The MAPbI<sub>3</sub> film obtained by

consecutively annealing at 65 °C for 1 min and at 100 °C for 9 min was used as reference. The  $\alpha$ -FAPbI<sub>3</sub> film obtained by annealing at 150 °C for 40 min was used as reference. To fabricate the hole transporting layer, 20  $\mu$ L of the spiro-MeOTAD solution (73.2 mg spiro-MeOTAD in 1 mL chlorobenzene including 28.8  $\mu$ L t-BP (tert-butylpyridine) and 17.5  $\mu$ L Li-TFSI solution (520 mg Li-TFSI in 1 mL acetonitrile (Sigma-Aldrich, 99.8%))) was spin-coated at 3000 rpm for 30 s. Finally, Ag electrode with a thickness of ca. 150 nm was deposited on top of the spiro-MeOTAD layer under  $4 \times 10^{-7}$  Torr using thermal evaporator. The as-fabricated PSCs were stored in the desiccator overnight before the current density-voltage (*J-V*) measurement.

**Characterizations.** *J-V* curves were recorded using a Keithley 2400 source meter under simulated one sun illumination (AM 1.5G, 100 mW/cm<sup>2</sup>) using a solar simulator (Oriel Sol 3A class AAA) equipped with 450 W Xenon lamp (Newport 6280NS), in which light intensity was adjusted by NREL-calibrated Si solar cell with KG-2 filter. Solar cells were covered with a metal mask with aperture area of 0.125 cm<sup>2</sup> during the measurement. External quantum efficiency (EQE) was measured by either an EQE system (PV measurement Inc.) equipped with a 75 W Xenon source lamp (USHIO, Japan) or a QuantX-300 Quantum Efficiency System (Newport) equipped with 100 W Xenon lamp. EQE data were collected at DC mode without bias light. The absorbance of the perovskite film was measured by UV-vis spectrometer (Lambda 45, Perkin-Elmer). Surface and cross-sectional morphologies were investigated by scanning electron microscope (SEM) (JSM-7600F, JEOL). X-ray diffraction (XRD) data were collected from a HP-thin film XRD-D8 Advance (Bruker), where Cu K $\alpha$  radiation was used ( $\lambda = 1.5406 \text{ \AA}$ ) and a scan rate was 2°/min. Steady-state

photoluminescence (PL) and time-resolved photoluminescence (TRPL) were measured using a fluorescence lifetime spectrometer (Quantaaurus-Tau C11367-12, Hamamatsu). Perovskite films were photo-excited with a 372 nm laser pulsed at the frequency of 10 MHz. The PL was detected by high sensitivity photon counting near IR detector. The cross-sectional morphologies and structures of the full cells were investigated using a high-resolution transmission electron microscope. The samples were prepared by vertical etching using focused ion beam (FIB) equipment (SMI3050TB). The cross-sectional surface was in-situ coated with platinum using the gas injection system (Zeiss CrossBeam) to protect the surface from damage during FIB milling. An FTO/SnO<sub>2</sub>/perovskite/spiro-MeOTAD specimen with approximately 40 nm in thickness was obtained. TEM images and SAED patterns were obtained using a high-resolution transmission electron microscope (JEOL JEM-2100F) at an acceleration voltage of 200 kV in the high-angle annular dark-field imaging mode. Trap density was estimated using SCLC (Space-Charge-Limited Current) method. Devices with the FTO/perovskite/Au layout were measured in the dark from 0 V to 1.5 V at the scan rate of 1000 ms. The observed response was analyzed according to SCLC theory. Trap density ( $n_t$ ) was estimated using the relation  $V_{\text{TFL}} = en_t d^2 / 2\epsilon\epsilon_0$ ,<sup>S2</sup> where  $V_{\text{TFL}}$  is the trap-filled-limit voltage,  $e$  is electron charge ( $1.602 \times 10^{-19}$  C),  $\epsilon$  is dielectric constant,  $\epsilon_0$  is the vacuum permittivity ( $8.8542 \times 10^{-14}$  F/cm) and  $d$  is the perovskite film thickness. The dielectric constant was calculated using the equation of  $\epsilon = Cd/A\epsilon_0$ , where  $C$  is capacitance at high frequency ( $\sim 10^4$  Hz) and  $A$  is area.<sup>S3,S4</sup>

***Molecular electrostatic potential.*** Molecular electrostatic potential (EP) was calculated using density functional theory (B3LYP/6-31G\*) for two cases of under vacuum or in DMF solvent.

The calculations were carried out by using Spartan'10 (Wavefunction, 2010) program. EP maps were obtained to present electrostatic charges, where electron-rich and electron-poor part was depicted as red and blue color, respectively.

**Density of state (DOS) and formation energy calculation.** For the density of states (DOS) and formation energy calculation, DFT calculations were performed with projector augmented wave (PAW) method<sup>S5</sup> and the revised Perdew, Burke, and Ernzerhof GGA (PBEsol)<sup>S6,S7</sup> for the exchange-correlation potential as implemented in Vienna Ab-initio Simulation Package (VASP) code.<sup>S8</sup>  $\alpha$ -FAPbI<sub>3</sub> has three formula units in a unit cell while  $\delta$ -FAPbI<sub>3</sub> has two formula units in a unitcell. So, the difference in finite cell size effect during charged system calculation is minimized by choosing 3×3×2 supercell for  $\alpha$ -FAPbI<sub>3</sub> and 3×3×3 supercell for  $\delta$ -FAPbI<sub>3</sub> in which both  $\alpha$ - and  $\delta$ -FAPbI<sub>3</sub> have identical system size of 54 formula units (648 atoms and 2916 electrons) in each supercell. The optimized lattice constants are  $a = 26.95 \text{ \AA}$  and  $c = 22.01 \text{ \AA}$  for  $\alpha$ -FAPbI<sub>3</sub> and  $a = 25.98 \text{ \AA}$  and  $c = 23.71 \text{ \AA}$  for  $\delta$ -FAPbI<sub>3</sub>. Periodic boundary condition and Monkhorst-Pack k-point sampling<sup>S9</sup> with a  $\Gamma$ -centred k-point grid of up to 2×2×2 was used for the Brillouin zone integration. An energy cutoff of 500 eV was used for the plane-wave representation of the wavefunctions and the 5d electrons of Pb were considered as valence electrons. Atomic structures were relaxed until all Hellman-Feynman forces were below 0.01 eV/Å. The formation energy is calculated by subtracting the energy of FAI and PbI<sub>2</sub> from the total energy of  $\alpha$ - or  $\delta$ -FAPbI<sub>3</sub>. Monoclinic and Rhombohedral crystal structure is used to calculate the energy of FAI (P2<sub>1</sub>/c) and PbI<sub>2</sub> (P3m1).

**Table S1.** TRPL curves fitting results obtained using bi-exponential decay equation  $y = y_0 + A_1 \exp(-t/\tau_1) + A_2 \exp(-t/\tau_2)$ , in which  $\tau_1$  is time constant for fast decay component and  $\tau_2$  is time constant for slow component. Effective lifetime was estimated from  $\tau_{\text{eff}} = A_1 \tau_1 / (A_1 + A_2) + A_2 \tau_2 / (A_1 + A_2)$ .

sample	$\tau_1$ (ns)	$A_1/(A_1+A_2)$	$\tau_2$ (ns)	$A_2/(A_1+A_2)$	$\tau_{\text{eff}}$ (ns)
MAPbI <sub>3</sub> -before	2.61	95.13%	245.80	4.87%	14.45
MAPbI <sub>3</sub> (F)-after	12.21	43.59%	537.34	56.41%	308.42
FAPbI <sub>3</sub> -before	36.45	62.75%	295.60	37.25%	132.98
FAPbI <sub>3</sub> -after	1.13	82.67%	428.53	17.33%	75.19
MAPbI <sub>3</sub> -before	2.83	97.81%	254.19	2.19%	8.34
MAPbI <sub>3</sub> (E)-after	7.22	96.59%	742.38	3.41%	32.30
EAPbI <sub>3</sub> -before*	-	-	-	-	-
EAPbI <sub>3</sub> -after	11.40	64.22%	286.61	35.78%	109.86

\*No decay signal

**Table S2.** Electrostatic potential of DMSO, MA<sup>+</sup>, FA<sup>+</sup> and EA<sup>+</sup> under vacuum or in DMF solvent.

Material	Atom	Vacuum (kJ/mol)	DMF (kJ/mol)
DMSO	O	-213.884	-249.755
DMSO	C	121.227	154.721
MA <sup>+</sup>	C	489.38	468.968
MA <sup>+</sup>	N	767.332	794.038
FA <sup>+</sup>	N(p) <sup>a</sup>	449.482	447.251
FA <sup>+</sup>	N-C-N <sup>b</sup>	739.214	743.479
EA <sup>+</sup>	C(2)	377.423	344.652
EA <sup>+</sup>	C(1)	468.243	455.742
EA <sup>+</sup>	N	740.704	789.012

<sup>a</sup>Electrons are localized on N

<sup>b</sup>Electrons are delocalized on the resonance structure of N-C-N

**Table S3.** Photovoltaic parameters of best performing devices based on the stamped MAPbI<sub>3</sub>, FAPbI<sub>3</sub> and reference films in the normal mesoscopic structure of FTO/bl-TiO<sub>2</sub>/mp-TiO<sub>2</sub>/perovskite/spiro-MeOTAD/Ag.

<b>Device</b>	<b>Scan direction</b>	<b><math>J_{sc}</math> (mA/cm<sup>2</sup>)</b>	<b><math>V_{oc}</math> (V)</b>	<b>FF</b>	<b>PCE (%)</b>	<b>Average PCE (%)</b>
MAPbI <sub>3</sub> -after	Reverse	21.820	1.126	0.788	19.36	15.20
	Forward	21.810	1.051	0.481	11.03	
MAPbI <sub>3</sub> -reference	Reverse	20.968	1.066	0.780	17.43	13.41
	Forward	21.156	1.040	0.427	9.39	
FAPbI <sub>3</sub> -after	Reverse	22.696	1.055	0.766	18.34	15.56
	Forward	22.679	0.975	0.578	12.78	
$\alpha$ -FAPbI <sub>3</sub> -reference	Reverse	22.642	1.080	0.705	17.24	16.15
	Forward	22.573	1.034	0.645	15.05	

**Table S4.** Photovoltaic parameters of best performing devices with MAPbI<sub>3</sub>, FAPbI<sub>3</sub> and EAPbI<sub>3</sub> films before and after stamping in the normal planar structure of FTO/SnO<sub>2</sub>/perovskite/spiro-MeOTAD/Ag.

Device	Scan direction	$J_{sc}$ (mA/cm <sup>2</sup> )	$V_{oc}$ (V)	FF	PCE (%)	Average PCE (%)
MAPbI <sub>3</sub> -before	Reverse	16.811	1.051	0.551	9.73	9.15
	Forward	16.624	1.432	0.494	8.57	
MAPbI <sub>3</sub> (F)-after	Reverse	22.022	1.126	0.814	20.18	17.73
	Forward	22.127	1.030	0.670	15.27	
FAPbI <sub>3</sub> -before	Reverse	0.379	0.312	0.252	0.03	0.03
	Forward	0.339	0.334	0.306	0.03	
FAPbI <sub>3</sub> -after	Reverse	21.840	1.062	0.766	17.76	17.40
	Forward	21.907	1.054	0.737	17.03	
EAPbI <sub>3</sub> -before	Reverse	0.202	0.268	0.250	0.01	0.02
	Forward	0.218	0.277	0.283	0.02	
EAPbI <sub>3</sub> -after	Reverse	18.600	1.071	0.654	13.02	12.14
	Forward	18.632	0.932	0.648	11.25	
MAPbI <sub>3</sub> (E)-after <sup>a</sup>	Reverse	20.871	1.096	0.722	16.52	14.49
	Forward	20.871	1.012	0.590	12.46	

<sup>a</sup>The J-V curve was not presented in the main text.

**Table S5.** Peak position and intensity of PL spectra for the EA<sub>1-x</sub>MA<sub>x</sub>PbI<sub>3</sub> perovskite films and the stamped EAPbI<sub>3</sub> film. The EA<sub>1-x</sub>MA<sub>x</sub>PbI<sub>3</sub> perovskite films were prepared from the solution containing (1-x)EAI and xPbI<sub>2</sub>.

EA <sub>1-x</sub> MA <sub>x</sub> PbI <sub>3</sub>	Peak1 (nm)	FWHM	Peak2 (nm)	Peak Intensity	FWHM
x = 0	486	13.7849	586	6290	-
x = 0.05	488	10.5686	684	14600	141.164
x = 0.10	488	11.1176	694	39620	107.779
x = 0.15	488	10.5816	694	113400	90.5275
x = 0.20	486	11.3713	740	262060	68.7557
x = 0.25	486	11.8086	746	309480	54.0379
x = 0.30	486	11.6415	750	216770	52.3104
x = 0.40	486	12.4091	752	232340	52.3964
x = 0.50	486	9.55349	758	124020	44.3932
Stamping	-	-	762	1155060	46.0027

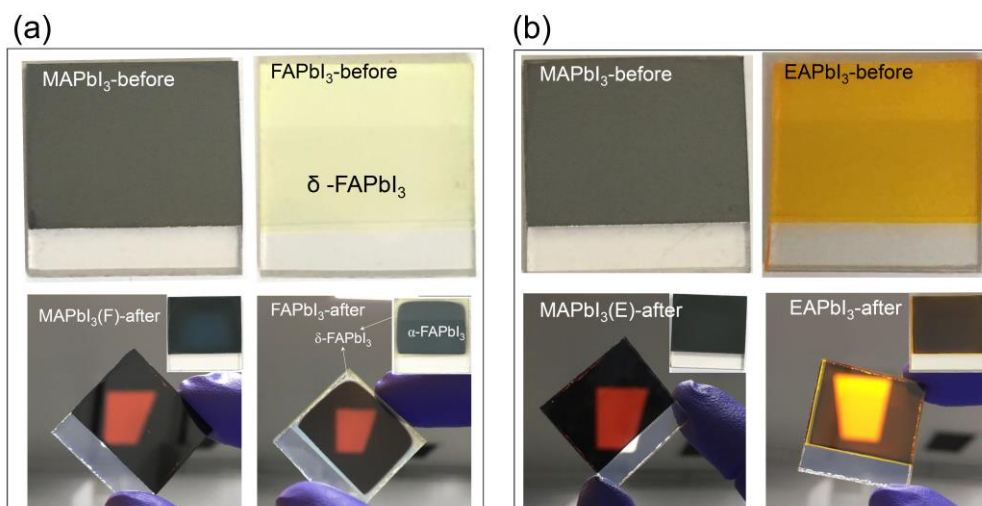


**Figure S1.** (a) Digital photographs of MAPbI<sub>3</sub> and FAPbI<sub>3</sub> before (up) and after (down) stamping method. (b) Digital photographs of MAPbI<sub>3</sub> and EAPbI<sub>3</sub> before (up) and after (down) stamping method. Insert images (down) are top view of the corresponding after stamping films.

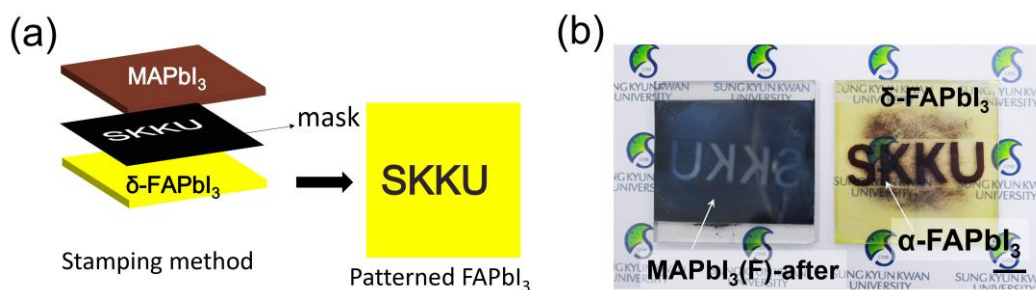


**Figure S2.** (a) Schematic illustration of fabricating process of “SKKU” letter patterned  $\alpha$ -FAPbI<sub>3</sub> on  $\delta$ -FAPbI<sub>3</sub> film. Insert “SKKU” mask between the MAPbI<sub>3</sub> and FAPbI<sub>3</sub> and then stamping. In the mask empty “SKKU” area, FAPbI<sub>3</sub> change the phase from  $\delta$  to  $\alpha$ -phase. (b) Photograph of “SKKU” patterned phase FAPbI<sub>3</sub> film on glass substrate (right) and the corresponding stamped MAPbI<sub>3</sub> film (left).

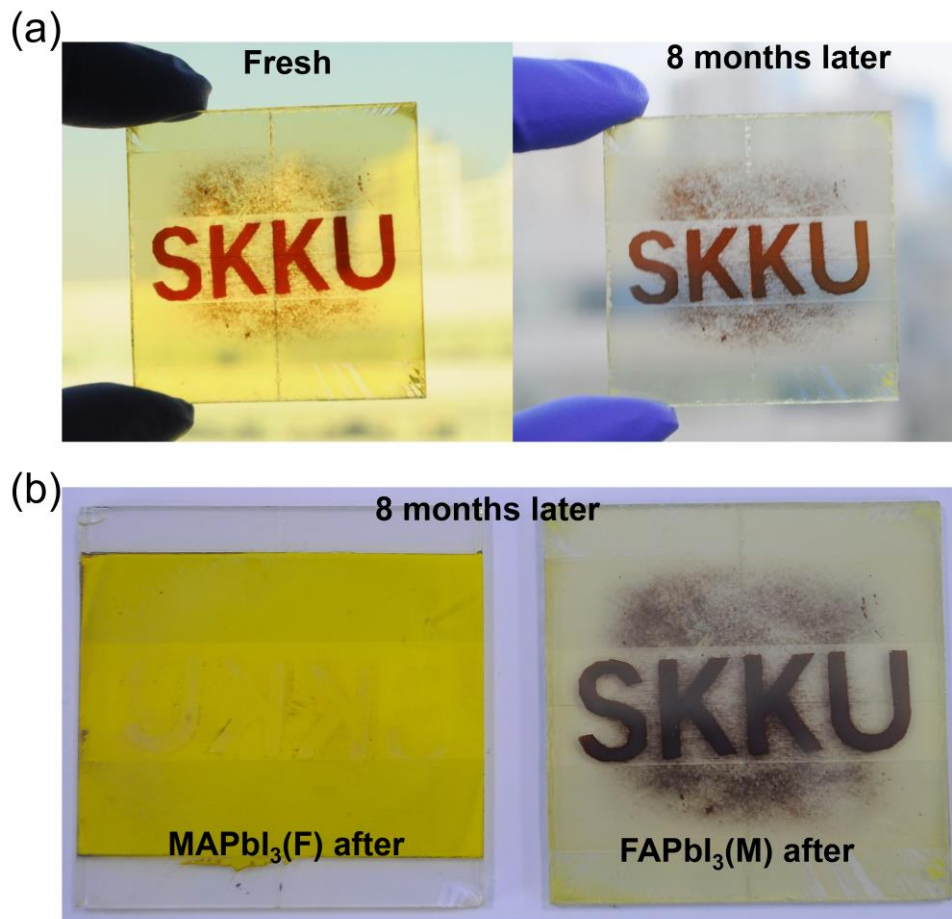
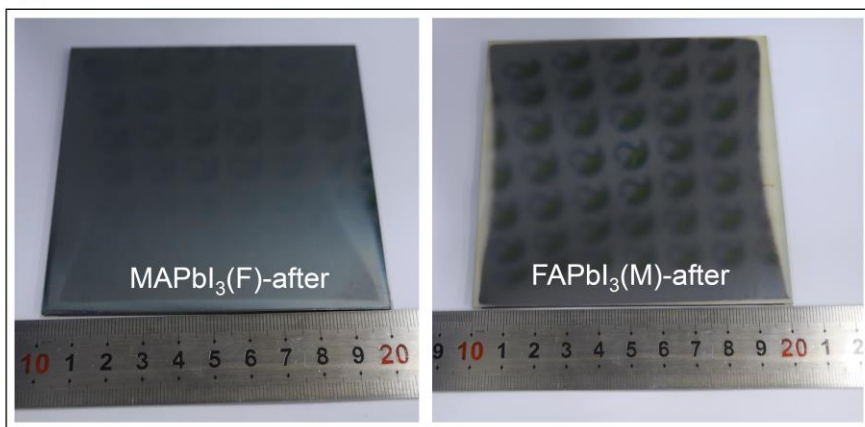


**Figure S3.** Digital photographs of (a) the as-prepared (left) and the 8-month-aged (right) FAPbI<sub>3</sub>(M)-after film. (b) Comparison of digital photographs of the 8-month-aged MAPbI<sub>3</sub>(M)-after (left) and FAPbI<sub>3</sub>(M)-after film. The films were stored in ambient condition with relative humidity of 30% ~ 40% and temperature of about 25 °C.

(a)



(b)

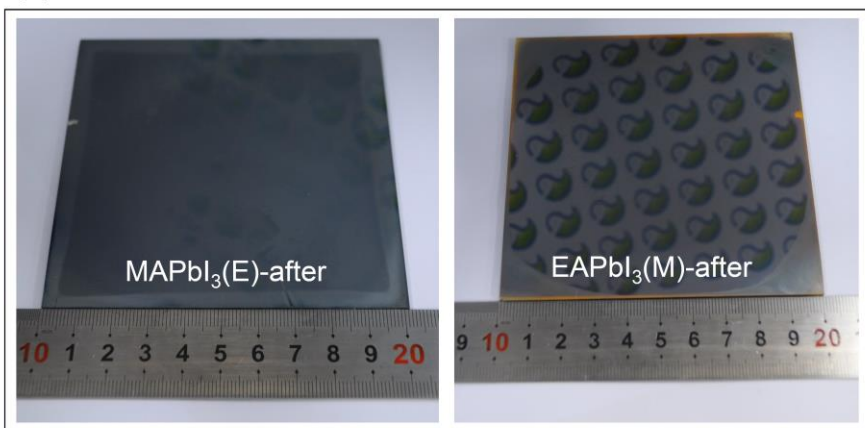


**Figure S4.** (a) Digital photographs of 10 cm×10 cm size MAPbI<sub>3</sub> film (left) stamped with FAPbI<sub>3</sub> film (right). (b) Digital photographs of 10 cm×10 cm size MAPbI<sub>3</sub> film (left) stamped with EAPbI<sub>3</sub> film (right). Stamping condition was the same as small size.

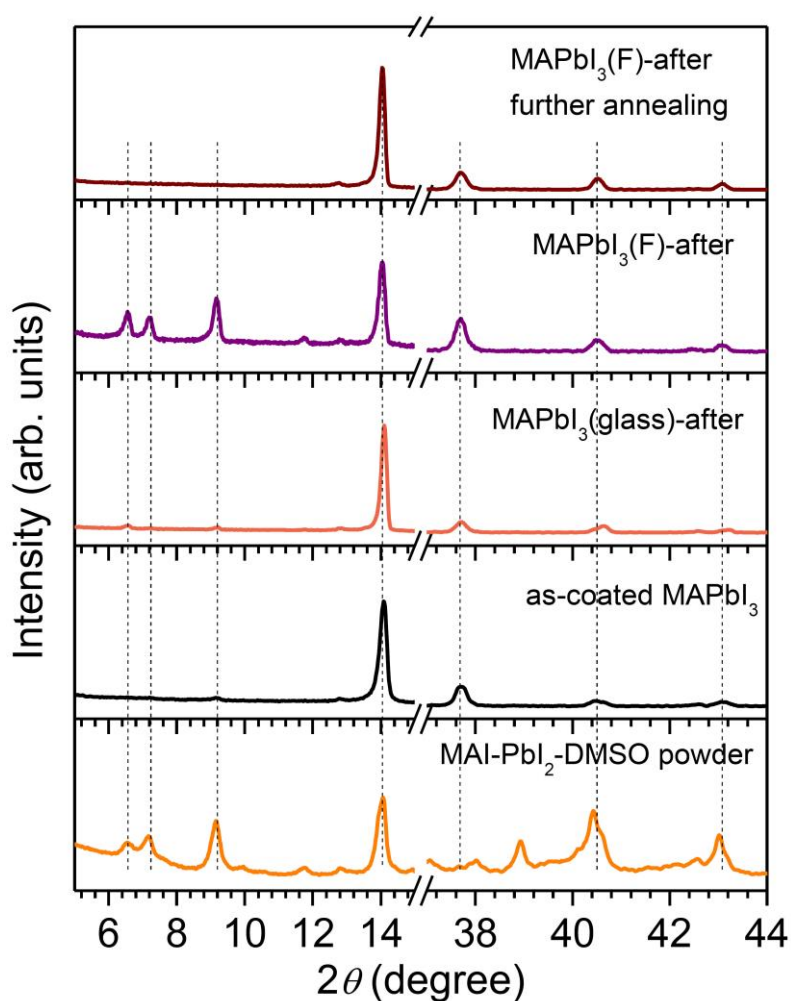


**Figure S5.** XRD patterns of MAI-PbI<sub>2</sub>-DMSO powder, as-coated MAPbI<sub>3</sub> film, MAPbI<sub>3</sub>(glass)-after, MAPbI<sub>3</sub>(F)-after and MAPbI<sub>3</sub>(F)-after-with-further-annealing. MAI-PbI<sub>2</sub>-DMSO powder was obtained by scratching and vacuum drying the MAPbI<sub>3</sub> adduct film. As-coated MAPbI<sub>3</sub> film represents as-coated MAPbI<sub>3</sub> film without annealing. MAPbI<sub>3</sub>(glass)-after stands for the MAPbI<sub>3</sub> film stamped with bare glass without counterpart perovskite film. MAPbI<sub>3</sub>(F)-after represents the MAPbI<sub>3</sub> film stamped with FAPbI<sub>3</sub> film. MAPbI<sub>3</sub>(F)-after-with-further-annealing was prepared by further annealing MAPbI<sub>3</sub>(F)-after film at 100 °C for 10 min.

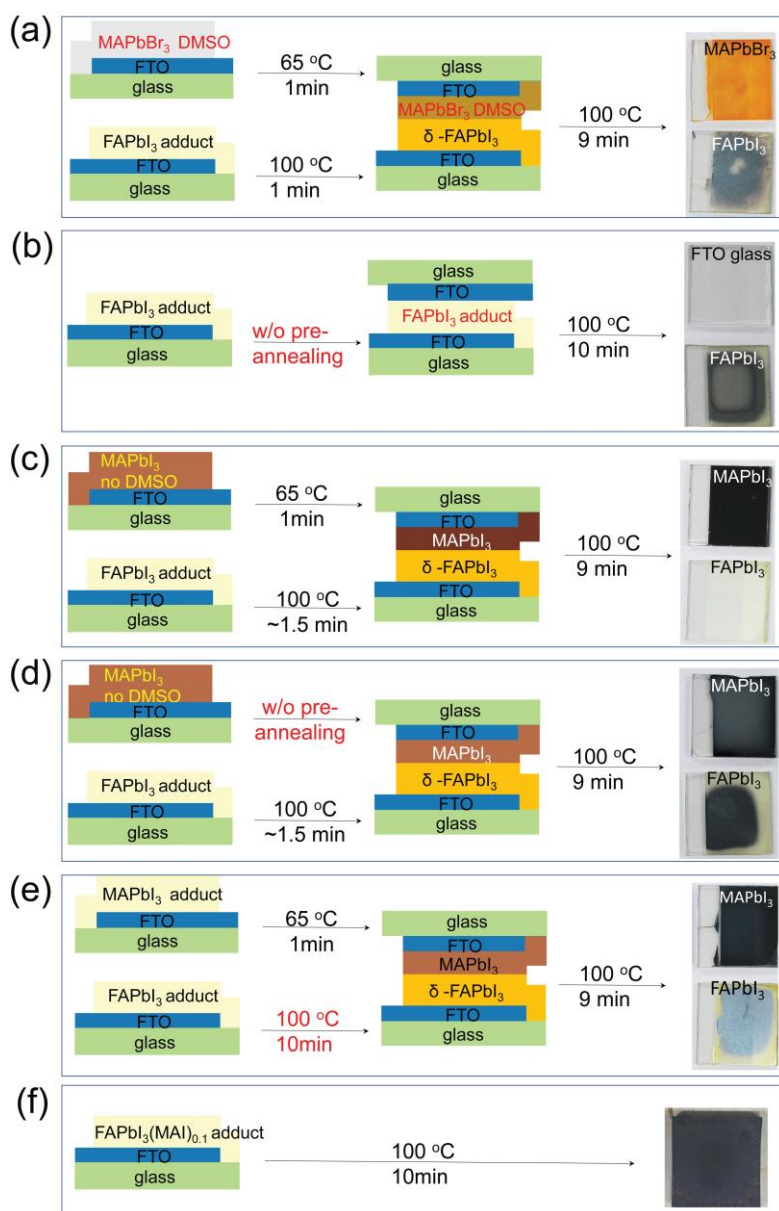


**Figure S6.** FAPbI<sub>3</sub> phase transition check after stamping with various films under different annealing conditions. Schematic illustration of different fabrication processes and counterpart perovskite materials along with digital photographs of the resulting films to verify the phase transition mechanism of FAPbI<sub>3</sub>. (a) MAPbBr<sub>3</sub>-DMSO adduct film prepared at 65 °C for 1 min was stamped with FAPbI<sub>3</sub>-before. (b) As-coated FAPbI<sub>3</sub> without pre-annealing was stamped with FTO glass. (c) MAPbI<sub>3</sub> film prepared from precursor solution without DMSO was stamped with FAPbI<sub>3</sub>-before. (d) Non-pre-annealed MAPbI<sub>3</sub> film prepared from precursor solution without DMSO was stamped with FAPbI<sub>3</sub>-before. (e) FAPbI<sub>3</sub>-before with longer annealing time of 10 min was stamped with MAPbI<sub>3</sub>-before. (f) FAPbI<sub>3</sub> film was fabricated from FAPbI<sub>3</sub> precursor solution with 0.1 mole excess MAI and annealed at 100 °C for 10 min. Except for (c),  $\delta \rightarrow \alpha$  phase transition occurred at all conditions.

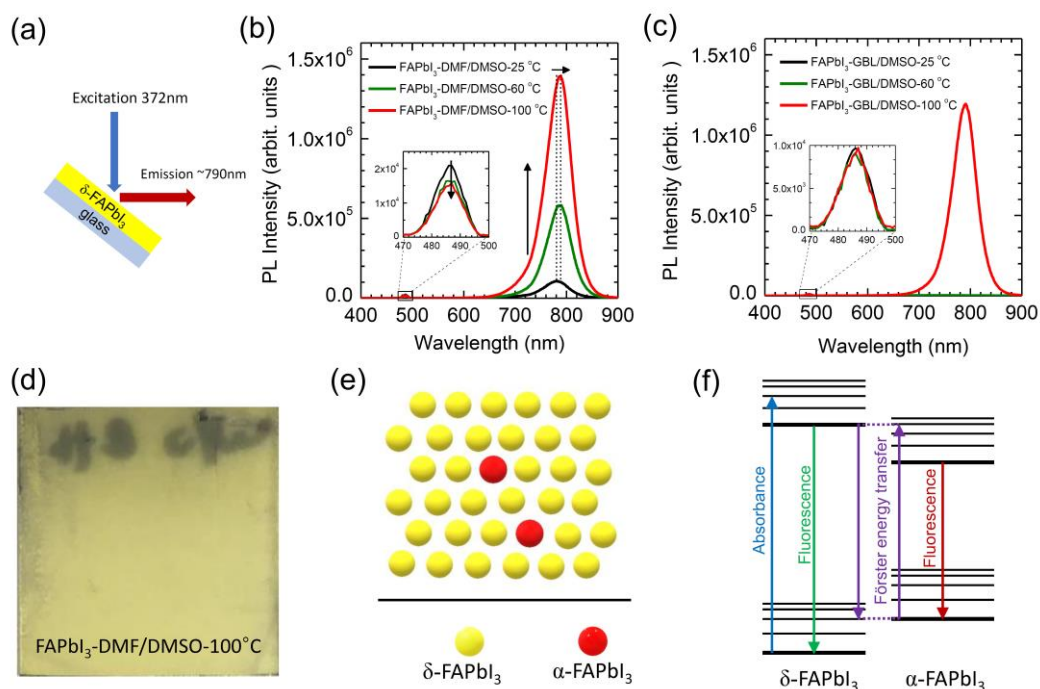


**Figure S7.** (a) PL measurement condition showing light was incident on perovskite side. (b) PL spectra of FAPbI<sub>3</sub> perovskite films obtained from the precursor solution in mixed DMSO/DMF system and annealing at 25 °C, 60 °C and 100 °C for 10 min. (c) PL spectra of FAPbI<sub>3</sub> perovskite films obtained from the precursor solution in mixed DMSO/ $\gamma$ -butyrolactone (GBL) system and annealing at 25 °C, 60 °C and 100 °C for 10 min. The perovskite films were fabricated using the Lewis acid-base adduct method according to the method.<sup>S1</sup> The excitation wavelength was 372 nm. (d) Digital photograph of 100 °C-annealed FAPbI<sub>3</sub> film from the precursor solution in DMSO/DMF. (e) Schematic illustration of host  $\delta$ -FAPbI<sub>3</sub> and dopant  $\alpha$ -FAPbI<sub>3</sub> based on film appearance observed in (d). (f) Förster resonance energy transfer from  $\delta$ -FAPbI<sub>3</sub> (donor) to  $\alpha$ -FAPbI<sub>3</sub> (acceptor).

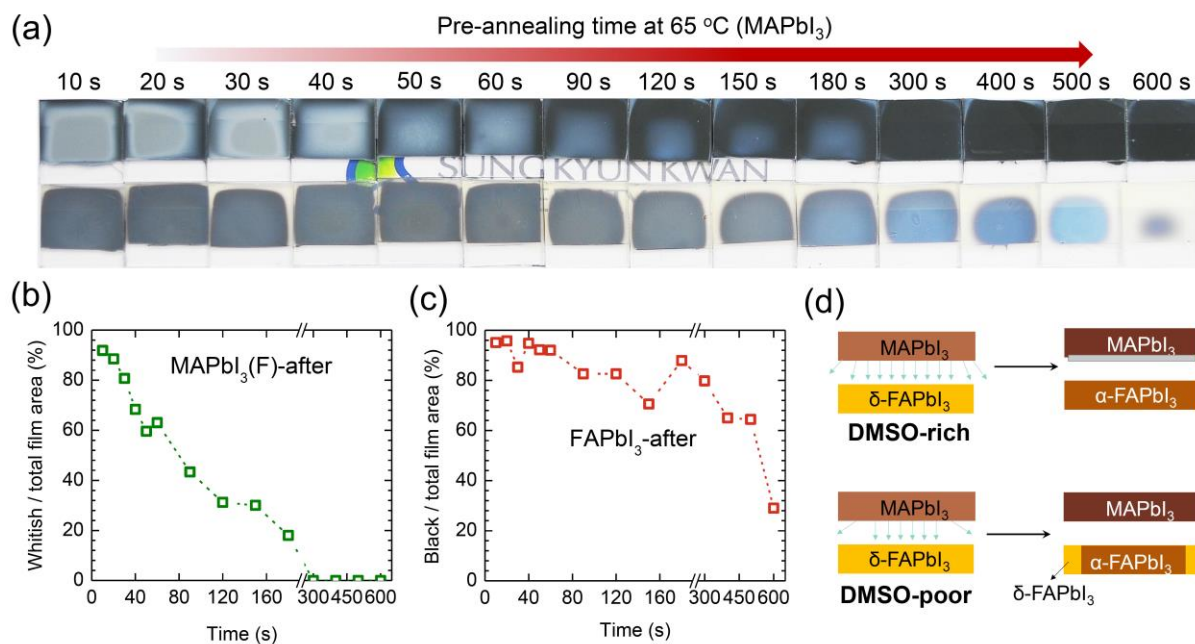


**Figure S8.** (a) Digital photographs of the stamped MAPbI<sub>3</sub> (up) and FAPbI<sub>3</sub> (down) films depending on the pre-annealing time of MAPbI<sub>3</sub>. (b) The ratio of whitish area to total area of MAPbI<sub>3</sub> film after stamping. (c) The ratio of black area to total area of FAPbI<sub>3</sub> film after stamping. (d) Schematic illustration showing the DMSO played important role in forming perovskite films during stamping process.

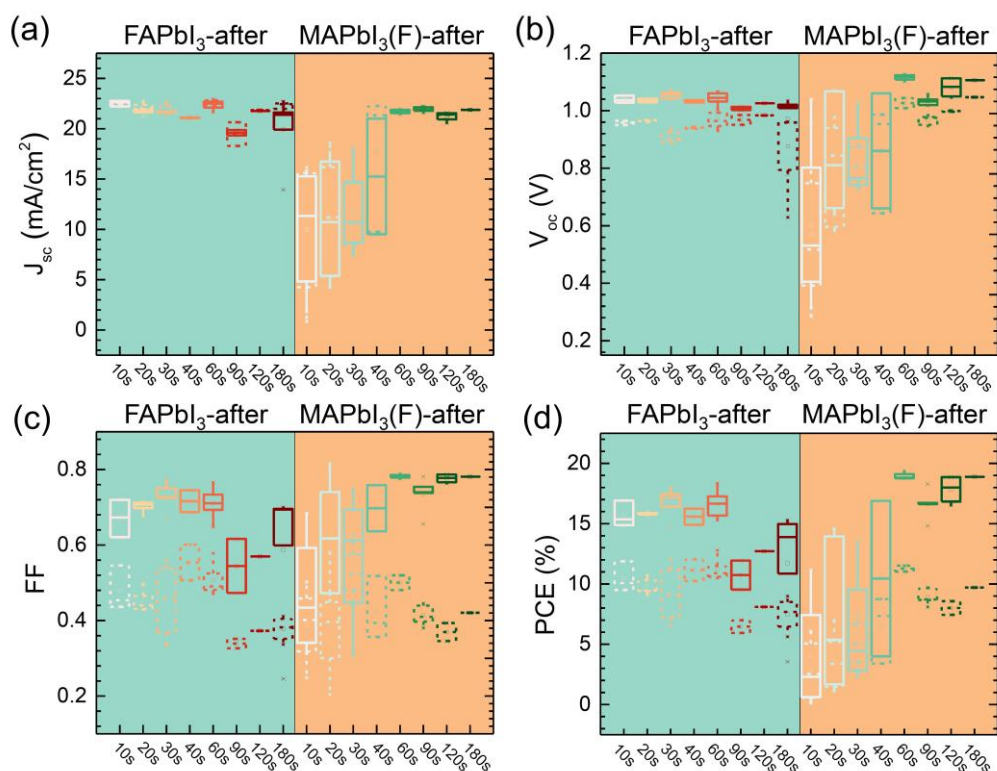


**Figure S9.** Statistic photovoltaic parameters of (a) current density ( $J_{sc}$ ), (b) open circle voltage ( $V_{oc}$ ), (c) fill factor (FF) and (d) power conversion efficiency (PCE) for the stamped MAPbI<sub>3</sub> and FAPbI<sub>3</sub> in normal mesoscopic structure. Pre-annealing time for MAPbI<sub>3</sub>-before was varied from 10 s to 180 s. The photovoltaic parameters were measured under AM 1.5G one sun illumination. Solid box and dashed box represent the data measured at reverse scan and forward scan, respectively. The scan rate was 0.13 V/s (voltage settling time of 200 ms).

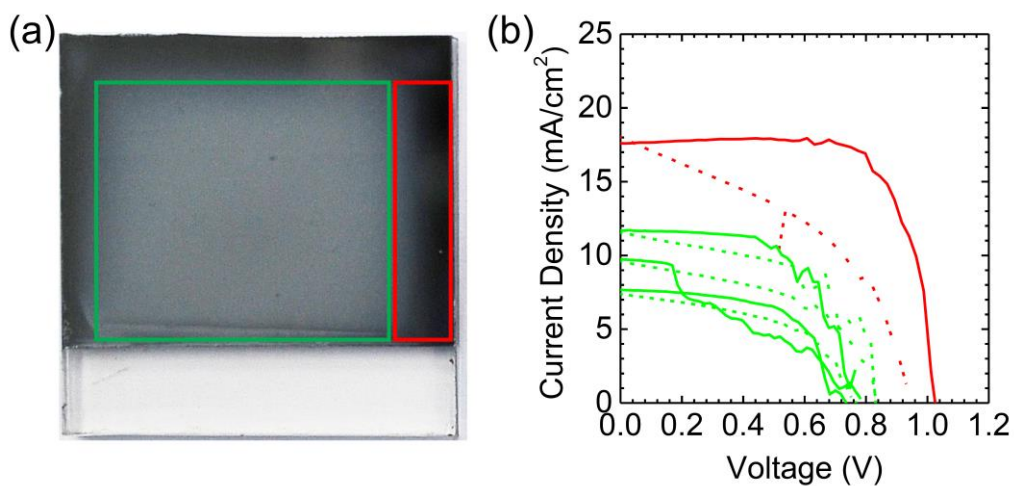


**Figure S10.** (a) Photograph of MAPbI<sub>3</sub> film after stamping with FAPbI<sub>3</sub>. Pre-annealing time for MAPbI<sub>3</sub>-before was 30 s. (b) *J-V* curves of the marked green and red area.

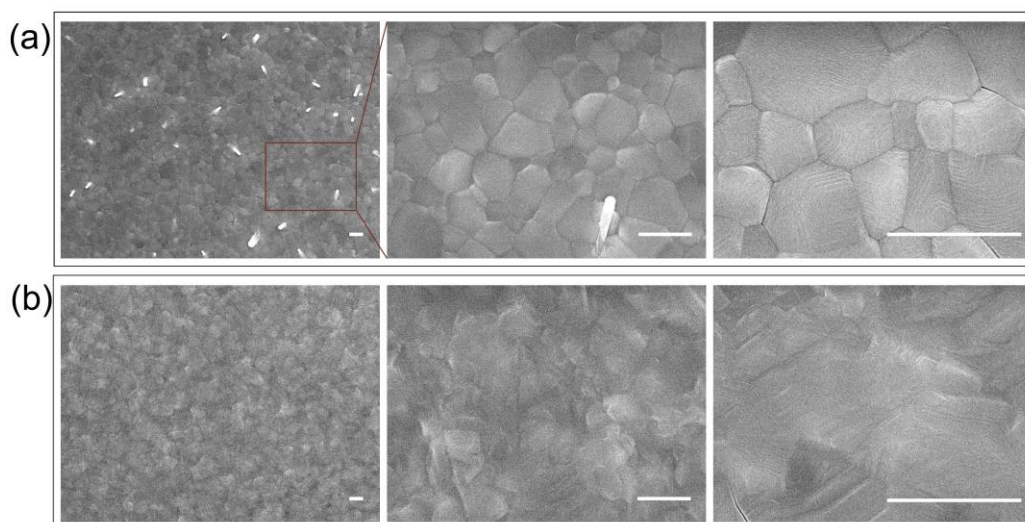


**Figure S11.** Top-view SEM images with different magnification (left to right, low to high magnification) for the stamped (a) MAPbI<sub>3</sub> and (b) FAPbI<sub>3</sub>. Pre-annealing time for MAPbI<sub>3</sub>-before was 30 s. Scale bars are 1  $\mu\text{m}$ .

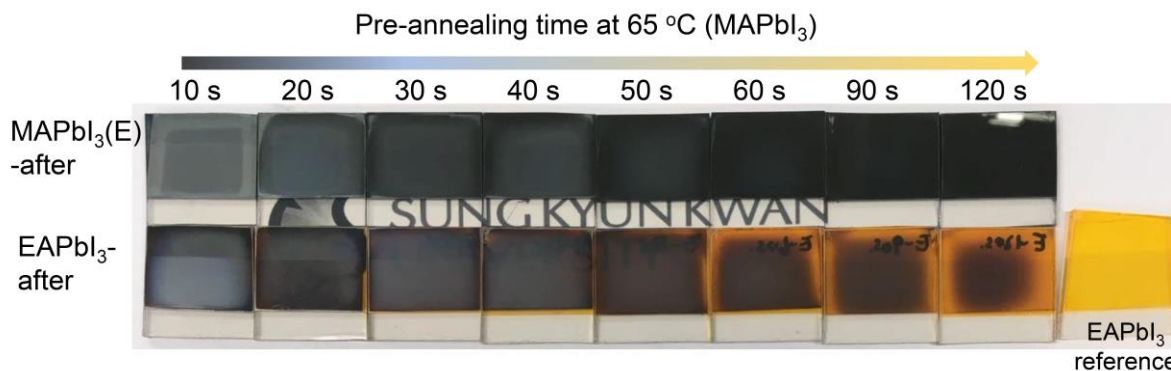


**Figure S12.** Photograph of the stamped MAPbI<sub>3</sub> (up) and EAPbI<sub>3</sub> (down) films depending on pre-annealing time of MAPbI<sub>3</sub>. EAPbI<sub>3</sub> reference film was obtained from annealing as-coated EAPbI<sub>3</sub> at 100 °C for 10 min without stamping.

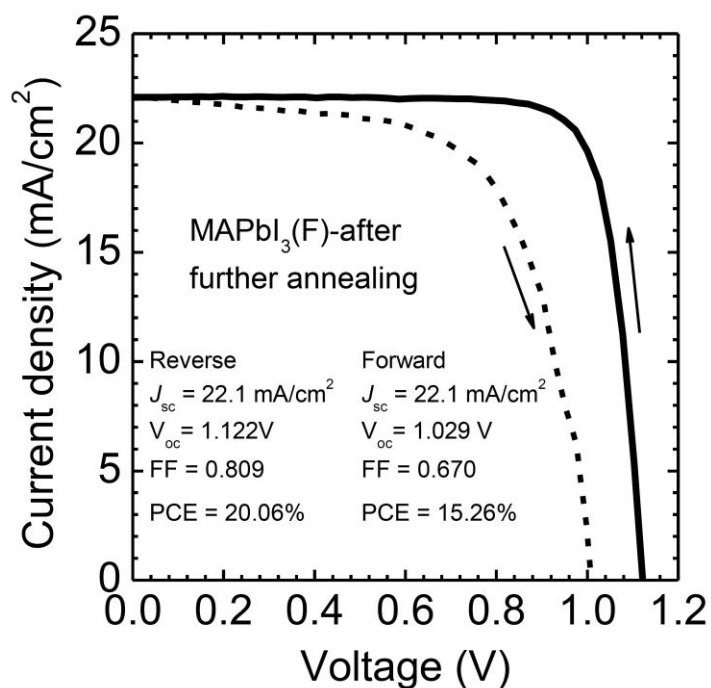


**Figure S13.** Reverse and forward scanned  $J$ - $V$  curves of PSC based on the MAPbI<sub>3</sub>(F)-after film further annealed at 100 °C for 10 min to eliminate the MAI-PbI<sub>2</sub>-DMSO phase. Device structure was glass/FTO/SnO<sub>2</sub>/perovskite/spiro-MeOTAD/Ag .

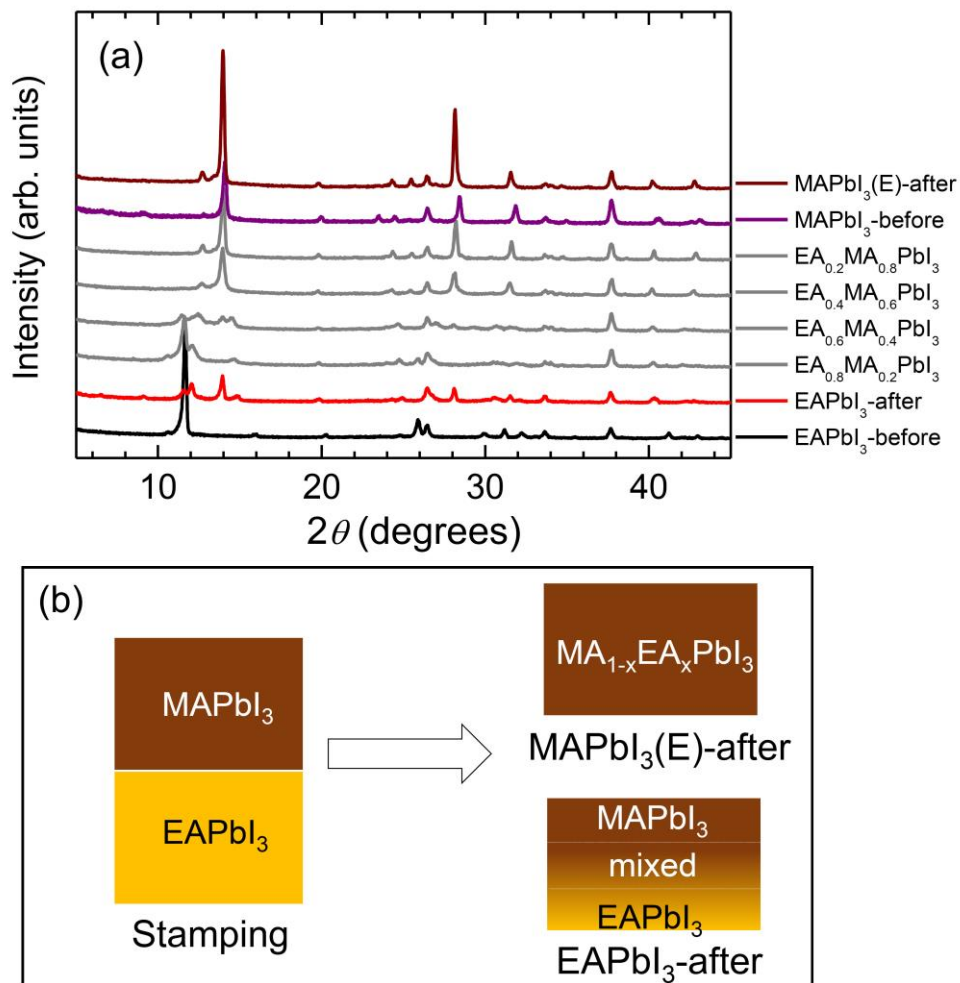


**Figure S14.** (a) XRD pattern of EAPbI<sub>3</sub> and MAPbI<sub>3</sub> before and after stamping, together with EA<sub>1-x</sub>MA<sub>x</sub>PbI<sub>3</sub>. EA<sub>1-x</sub>MA<sub>x</sub>PbI<sub>3</sub> films were prepared by mixing (1-x)EAI and xMAI in PbI<sub>2</sub> in DMSO/DMF co-solvent, spin-coating the precursor solution and then annealing at 100 °C for 10 min without stamping. (b) Schematic compositional change after stamping via ion exchange during stamping process.

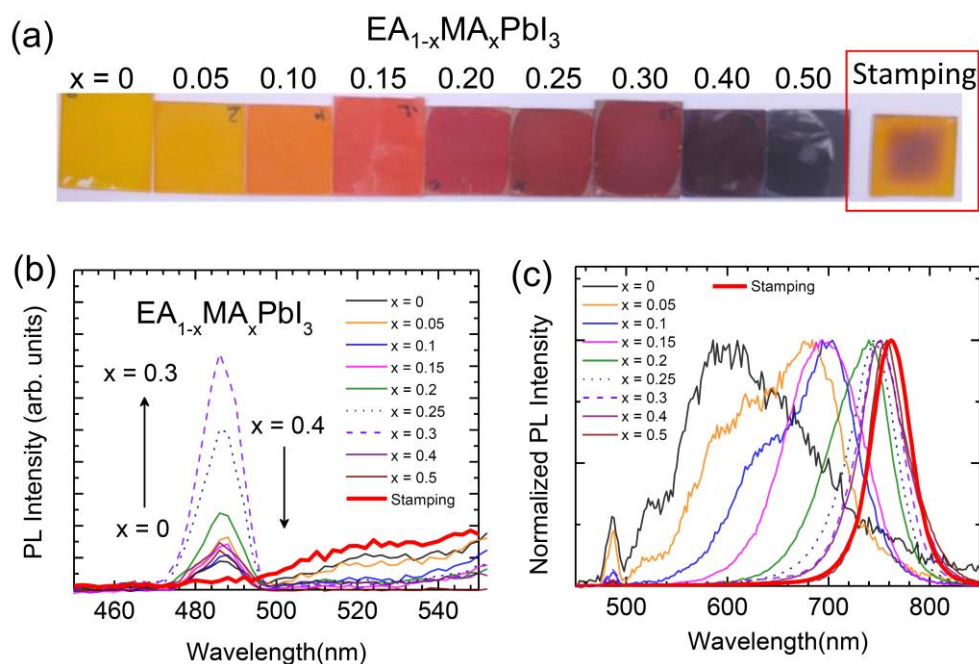


**Figure S15.** (a) Digital photographs of perovskite films based on  $EA_{1-x}MA_xPbI_3$  and stamped  $EAPbI_3$ . (b) Steady-state PL in the short wavelength region and (c) normalized PL in the long wavelength region for perovskite films based on  $EA_{1-x}MA_xPbI_3$  and stamped  $EAPbI_3$ . The excitation wavelength was 372 nm.

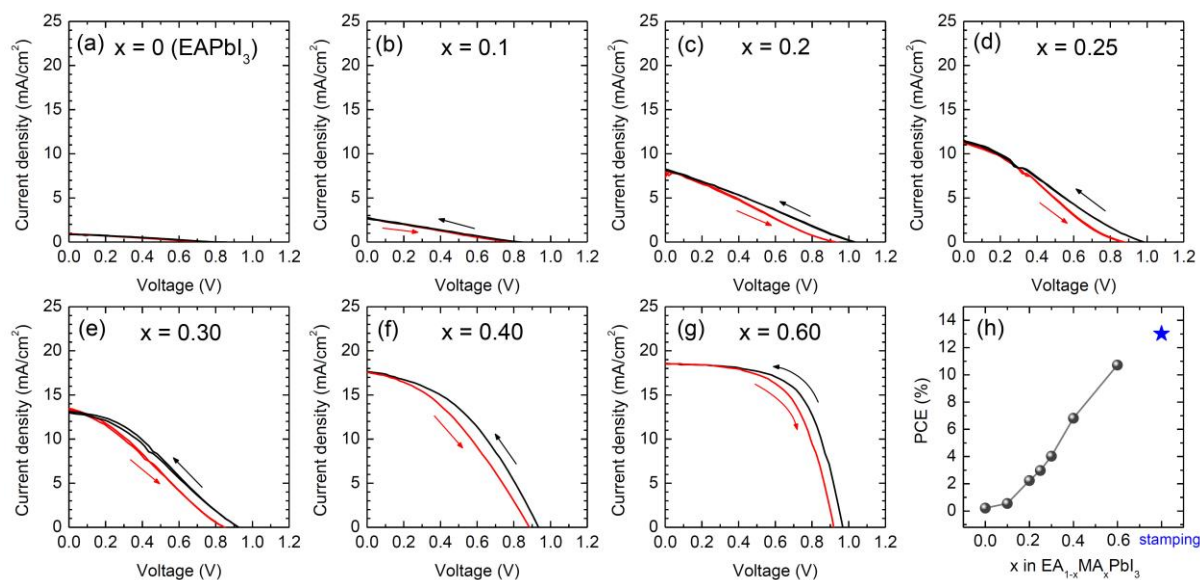


**Figure S16.** Reverse and forward scanned  $J-V$  curves of PSCs with the structure of FTO/SnO<sub>2</sub>/perovskite/spiro-MeOTAD/Ag based on  $EA_{1-x}MA_xPbI_3$  perovskite films with (a)  $x = 0$ , (b)  $x = 0.10$ , (c)  $x = 0.20$ , (d)  $x = 0.25$ , (e)  $x = 0.30$ , (f)  $x = 0.40$  and (g)  $x = 0.60$ . (h) PCE plot with respect to  $x$  in  $EA_{1-x}MA_xPbI_3$  along with PCE (star) for the stamped  $EAPbI_3$ .

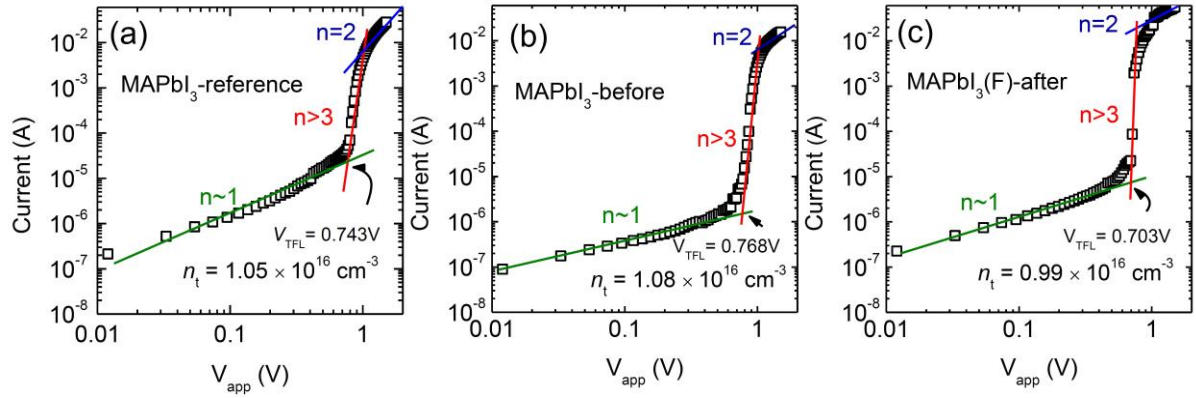


**Figure S17.** Dark current-voltage curve of the device (FTO/perovskite/Au) with (a) reference MAPbI<sub>3</sub> (annealing at 65 °C for 1 min and then at 100°C for 9 min without stamping), (b) MAPbI<sub>3</sub> before stamping and (c) MAPbI<sub>3</sub> after stamping with FAPbI<sub>3</sub>. Trap density ( $n_t$ ) was estimated from the equation  $V_{\text{TFL}} = en_t d^2 / 2\epsilon\epsilon_0$ , where  $V_{\text{TFL}}$  is the trap-filled-limit voltage,  $e$  is the electric charge ( $1.602 \times 10^{-19}$  C),  $\epsilon$  is the dielectric constant,  $\epsilon_0$  is the vacuum permittivity ( $8.8542 \times 10^{-14}$  F/cm) and  $d$  is the film thickness.

## Supporting Information References

S1. Ahn, N.; Son, D.-Y.; Jang, I.-H.; Kang, S. M.; Choi, M.; Park, N.-G. Highly Reproducible Perovskite Solar Cells with Average Efficiency of 18.3% and Best Efficiency of 19.7% Fabricated via Lewis Base Adduct of Lead(II) Iodide. *J. Am. Chem. Soc.* **2015**, *137*, 8696-8699.

S2. Rose, A. Space-Charge-Limited Currents in Solids. *Phys. Rev.* **1955**, *97*, 1538-1544.

S3. V., B. V.; Ko, K. A. K.; D., M. P.; Jie, Z. Quantifying Interface States and Bulk Defects in High-Efficiency Solution-Processed Small-Molecule Solar Cells by Impedance and Capacitance Characteristics. *Prog. Photovolt. Res. Appl.* **2015**, *23*, 1526-1535.

S4. Zhumekenov, A. A.; Saidaminov, M. I.; Haque, M. A.; Alarousu, E.; Sarmah, S. P.; Murali, B.; Dursun, I.; Miao, X.-H.; Abdelhady, A. L.; Wu, T.; Mohammed, O. F.; Bakr, O. M. Formamidinium Lead Halide Perovskite Crystals with Unprecedented Long Carrier Dynamics and Diffusion Length. *ACS Energy Lett.* **2016**, *1*, 32-37.

S5. Blöchl, P. E. Projector Augmented-Wave Method. *Phys. Rev. B* **1994**, *50*, 17953-17979.

S6. Perdew, J. P.; Burke, K.; Ernzerhof, M. Generalized Gradient Approximation Made Simple. *Phys. Rev. Lett.* **1996**, *77*, 3865-3868.

S7. Perdew, J. P.; Ruzsinszky, A.; Csonka, G. I.; Vydrov, O. A.; Scuseria, G. E.; Constantin, L. A.; Zhou, X.; Burke, K. Restoring the Density-Gradient Expansion for Exchange in Solids and Surfaces. *Phys. Rev. Lett.* **2008**, *100*, 136406.

S8. Kresse, G.; Furthmüller, J. Efficiency of Ab-Initio Total Energy Calculations for Metals and Semiconductors Using a Plane-Wave Basis Set. *Comput. Mater. Sci.* **1996**, *6*, 15-50.

S9. Monkhorst, H. J.; Pack, J. D. Special Points for Brillouin-zone Integrations. *Phys. Rev. B* **1976**, *13*, 5188-5192.